Matrix isolation infrared study and *ab initio* calculations for Borazine – Water complexes

PIYUSH MISHRA

MS10106

A dissertation submitted for the partial fulfilment of BS-MS dual degree in Science

Indian Institute of Science Education and Research Mohali

April 2015

Certificate of Examination

This is to certify that the dissertation titled "Matrix Isolation Infrared Study and Computational Calculations for borazine-water complexes" submitted by Piyush Mishra (Reg. No. MS10106) for the partial fulfilment of BS-MS dual degree programme of the Institute, has been examined by the thesis committee appointed by the Institute. The committee finds the work done by the candidate satisfactory and recommends that the report be accepted.

Prof. K. S. Viswanathan **Dr. P. Balanarayan** **Dr. Sugumar Venkataramani**

(Supervisor)

Dated: 24th April, 2015

DECLARATION

The work presented in this dissertation has been carried out by me under the guidance of Prof. K. S Viswanathan at the Indian Institute of Science Education and Research Mohali.

This work has not been submitted in part or in full for a degree, a diploma, or a fellowship to any other university or institute. Whenever contributions of others are involved, every effort is made to indicate this clearly, with due acknowledgement of collaborative research and discussions. This thesis is a bonafide record of original work done by me and all sources listed within have been detailed in the bibliography.

Piyush Mishra

Dated: 24th April, 2015

In my capacity as the supervisor of the candidate's project work, I certify above statements by the candidate are true to the best of my knowledge.

Prof. K.S. Viswanathan

(Supervisor)

ACKNOWLEDGEMENTS

I am very grateful to my masters thesis supervisor Prof. K. S. Viswanathan for his guidance, valuable suggestions and constant support throughout the course of this project.

I am also thankful to my thesis committee members Dr. P. Balanarayan and Dr. Sugumar Venkataramani for their valuable comments on my project.

I owe a special word of thanks to Dr. Sanjay Singh and Mr. Deependra Bawari for carrying out the synthesis of borazine.

I am very thankful to Ms Kanupriya Verma, to continually help me during my project work. I am also thankful to my lab members Mr Akshay Raut, Ms Gargi Jagdale, Ms Ginny Karir, Ms Jyoti Saini, and Mr Pankaj Dubey for their constant support during the project work and their critical remarks. The entire experience has been enjoyable because of them.

List of figures

List of tables

CONTENTS Page No.

Chapter 1

Introduction

1.1 About borazine and its applications

Borazine (Fig. 1) is an important industrial compound as it is the precursor for the preparation of boron nitride [1-3]. Boron nitride has many important properties such as high temperature stability, strength, low chemical reactivity, corrosion resistance, electrical resistivity and thermal conductivity which makes it industrially important [4, 5]. Even though BN can be obtained in powdered form easily without the use of borazine as precursor [6], the use of borazine to form boron nitride is the method of choice when we need boron nitride in the form of coatings, fibres or intricate body shapes [7-9].

Handling borazine is very difficult. Borazine has high vapour pressure (~260 mmHg at 25°C) [10] which is almost ten times that of water (~24 mmHg at 25 ^{o}C) [11]. And it is very unstable in ambient conditions. It is extremely sensitive to moisture and decomposes fairly rapidly in presence of water.

Understanding borazine and its interaction with water is therefore very important. The motivation of the present work was to understand the nature of the non-covalent interaction in the borazine-water system. It was also thought interesting to compare the borazine-water system to the benzene-water system, which is also the motivation of the present work.

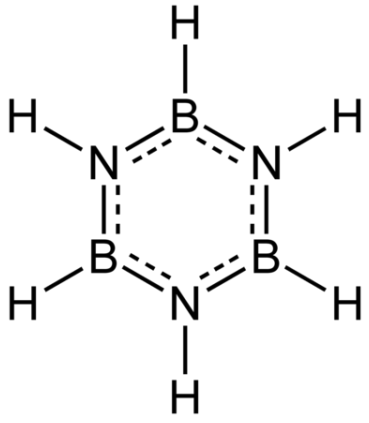

Figure 1: Borazine

1.2 Hydrogen bond

Hydrogen bonding is extremely important and fundamental to a very large number of processes. It is weaker than a covalent or an ionic bond. It is a strong electrostatic attraction between two dipoles. IUPAC had formed a task group in 2011, which had experts from different parts of the world, to give the modern definition of hydrogen bond [12].

"The hydrogen bond is an attractive interaction between a hydrogen atom from a molecule or a molecular fragment X–H in which X is more electronegative than H, and an atom or a group of atoms in the same or a different molecule, in which there is evidence of bond formation".

It is responsible for formation of DNA double helical structure, protein folding, many unique properties of water etc. which are vital for the existence of life [13-17]. This bond is seen in all three states of matter in ambient conditions. Study of hydrogen bonded complexes is crucial to understand many interactions and reactions around us.

When a hydrogen bond is formed between H covalently bonded to electronegative X and electronegative group Y represented as the following: X–H…Y, a decrease of X–H stretching frequency is observed [17, 18]. This red shift is a very important characteristic of hydrogen bonded interaction. There is a partial transfer of electron density from the proton acceptor's lone pair to the proton donor's sigma antibonding orbital [19]. This is the reason why a weakening and elongation of the X-H bond is seen ultimately resulting in decrease in the stretching frequency. On the contrary, it is also seen that X–H bond gets compressed in a hydrogen bonding unlike what was observed before. The corresponding X–H stretching vibration was blue shifted i.e. shifted to a higher frequency. This type of hydrogen bond is called improper or blue shifting or anti-H bonding.

1.3 Theme of the present project

In this work, we attempted to understand the complexes of borazine and water using the technique of matrix isolation infrared spectroscopy. The inert gases used in this work to prepare the solid matrix were nitrogen and argon at temperatures around 12 K. The main advantage of this technique is the significantly reduced linewidths compared with those obtained in conventional solid and liquid infrared spectra. The reduction in linewidths results

from the suppression of rotational congestion, reduction in linewidths arising from collisional and Doppler broadening. Furthermore, the molecules of interest are deposited at very high dilutions, so that they are trapped isolated from each other. Complex formation is then promoted by warming the matrix to about 30-35 K, holding it at the elevated temperature for sometime, typically 30 to 60 min, and the recooling the matrix back to 12 K. The process referred to as annealing encourages complex formation between the trapped precursors, which are indicated as new product bands in the infrared spectra.

Borazine has two sites that can form hydrogen bonded complexes with water N-H group can serve as a proton donor while the nitrogen can serve as a proton acceptor. Likewise water has two potential sites for hydrogen bonded interaction. It was therefore interesting to probe the preferences in the use of these sites, in hydrogen bond formation and the reasons thereof.

Boron exists in two isotopic forms. ^{11}B is 80.1% abundant and ^{10}B is 19.9% abundant [20]. All vibrational modes involving the excursions of boron, can be expected to show an isotopic splitting. The relative intensities of the peak that are split will depend upon the relative abundances of the isotope. Consequently, four isotopomers of borazine can be seen with relative abundances of 0.007 ($^{10}B^{10}B^{10}B$), 0.095 ($^{10}B^{10}B^{11}B$) , 0.383 ($^{10}B^{11}B^{11}B$) and 0.514 ($^{11}B^{11}B^{11}B$).

Chapter 2

Experimental setup and procedure

2.1 About matrix isolation

Matrix isolation is a technique where the sample molecules to be studied are trapped in inert gas solids at very low temperatures (~12 K). The molecules of interest are isolated in this rigid matrix at a typical matrix to sample ratios of 1000:1.

This technique was originally developed to trap transient and reactive species such as free radicals. The idea of matrix isolation was first proposed and later developed by Pimentel and co-workers during the mid 1950s [21]. They intended to study free radicals, as these reactive species have long lifetimes in the inert matrix. It was also realised that this technique could yield linewidths that were small due to the absence of rotational fine structures and Doppler and collision broadening.

2.2 Matrix effects and characteristics

Advantages and challenges of using matrix isolation

In the matrix, molecules can be isolated in substitutional sites or interstitial sites. Matrix does not chemically react with the sample molecules, but the packing and other physical effects show up in the spectra in form of multiplets which result from the immediate environment of matrix molecules around the sample to be different which in turn affects the vibration frequencies. These sites vary in stability, and in order to remove the unstable and sharpen the vibrational features, annealing is resorted to. Sometimes degenerate vibrational bands also are split due to lower symmetry in the matrix cage.

In a very small number of cases, small molecules, such as water and ammonia, have been observed to execute rotations in the matrix [22]. However, by and large, rotations are quenched in the low temperature solid inert gas matrix.

Typically the concentration ratio of matrix to sample is 1000:1 which ensures isolation, but as the sample's relative concentration is increased, features of dimers, trimers and higher multimers have been observed. While the features due to the higher clusters can lead to complications in the spectral assignments, they are usually identified by carrying out concentration and temperature variation in experiments.

Isolation of sample molecules in the matrix is ensured by adopting high dilutions of the samples in the inert gas mixture. The probability of isolation can be calculated using simple rules of probability. For example, for a molecule of carbon monoxide, occupying a single substitutional site, the probability of intermolecular interaction can be found. It is the chance of another CO molecule occupying one of the 12 sites around the original CO molecule that form the cage. The probability for absence of another CO molecule around the original CO is the following formula: $P = (1-r)^{12}$. Here r is the reciprocal of the matrix ratio. If r is very small, the expression can be written as $P = (1-12r)$. From this it is more clear as to why we need the matrix to sample ratio to be 1000:1to ensure 99% isolation.

Shifts due to matrix effects

Matrix shifts refer to frequency shifts seen from the gas phase sample molecules when trapped in matrix which arises due to four major factors: electrostatic ($\Delta \nu_{elec}$), inductive ($\Delta \nu_{ind}$), dispersive ($\Delta\nu_{dis}$) and repulsive interactions ($\Delta \nu_{rep}$) and is given by the following expression [23]

$$\Delta\nu = (\nu_{matrix} - \nu_{gas}) = \Delta \nu_{elec} + \Delta \nu_{ind} + \Delta \nu_{dis} + \Delta \nu_{rep} \quad \text{(eq. 1)}$$

Here ν_{matrix} is the frequency of sample in matrix and ν_{gas} is the frequency of the sample molecule in the gas phase.

In inert gases such as nitrogen and argon small shifts are seen. The electrostatic interaction is absent. In such systems ,the two dominant forces are dispersion forces and short range repulsion. Theoretically it had been found that tight cages cause blue shift and loose cages cause red shift in vibrational frequencies [24].

Perturbation due to solvent causes frequency shifts in sample that is given by Buckingham expression [25],

$$\Delta \nu = (\nu_{solvent} - \nu_{gas}) = [B_e/hc\omega_e] [U'' - 3AU'/\omega_e) \quad \text{(eq. 2)}$$

Here, $B_e = h/8\pi^2\mu c r_e^2$, is the rotational constant, $U' = \{\delta U/\delta r_{bc}\}$ and $U'' = \{\delta^2 U/\delta r_{bc}^2\}$
A is the anharmonicity constant, $c\omega e$ is the harmonic oscillator frequency for the normal vibration, Q.

The blue shift and red shift due to matrix cage can be understood with the help of the potential energy diagram shown in figure 2. This is a polyatomic molecule trapped in matrix. R_{CM} is the distance between matrix molecule and the sample molecule.

Case 1: Red shift occurs when R_{CM} is greater than R_1. Then U, U' and U'' are all negative, i,e, attractive. This can be understood by looking at equation 2 above. In this case $\Delta \nu$ is negative. This is a loose cage around the sample molecule.

Case 2: Blue shift occurs when R_{CM} is less than R_e (equilibrium distance). Then U' and U'' are both negative. This can be understood by looking at equation 2 above. In this case $\Delta \nu$ is positive. This is a tight cage around the sample molecule.

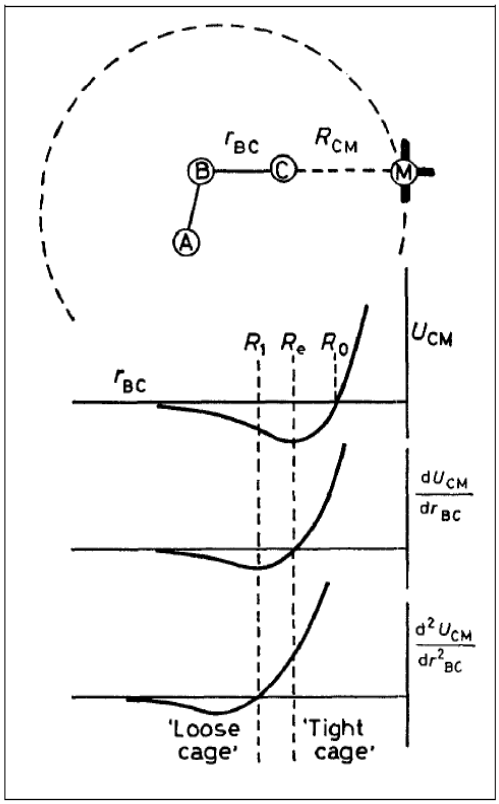

Figure 2: Loose cage and tight cage effects on the frequency shifts of the sample molecule.

(Source: Hallam, H. E. *Vibrational Spectroscopy of Trapped Species* (Wiley Inter science Publication, London, 1973)

Matrix material requirements

There are many important characteristics and properties that need to be considered for an inert gas to be used as a matrix. Nitrogen and noble gases except helium are used as matrix material.

Inertness - needed for minimal sample-matrix interaction. Among noble gases, due to increase in polarisability down the group, its reactivity increases.

Rigidity - this is required to ensure that no diffusion and readjustment takes place once the matrix is formed. The temperature of the matrix must not be more than one third of the melting point of the matrix. It is 26 K for N_2, 9 K for Ne, 29 K for Ar, 40 K for Kr and 55 K for Xe [23].

Transperancy - the matrix has to be transparent to the incident light. It should be absorption free and must not scatter the light much. The problem that is faced is that scattering is more at lower temperature as during deposition of the matrix the gas experience rapid cooling hence resulting in imperfect crystal formation.

Volatility - at room temperature, the vapour pressure has to be enough to ensure proper mixing with the sample. And at low temperatures it must be rigid enough to ensure isolation is maintained.

Rate of diffusion – the latent heat of fusion and thermal conductivity of matrix have no effect on diffusion of sample molecules, but the rate of deposition needs to be controlled to avoid rise in temperature of the matrix. According to Moskovits and Ozin, temperature increases as the square of rate of deposition and increases linearly with time. The gases mentioned above that are used in matrix form face-centered cubic (fcc) lattices at the temperatures at which we are working. Depending on the size of the sample molecule the number of substitutions vary, i.e. the number of matrix molecules displaced to accommodate one sample molecule [23]. There are also interstitial sites like tetrahedral voids and octahedral voids to accommodate sample molecules. But only small molecules occupy interstitial sites [23].

2.3 Instrumentation

The matrix isolation infrared spectroscopy set-up in our lab is shown in figure 3. The mixing chamber and the double jet effusive nozzles that open to the cryostat window are shown in figure 4 and figure 5 respectively.

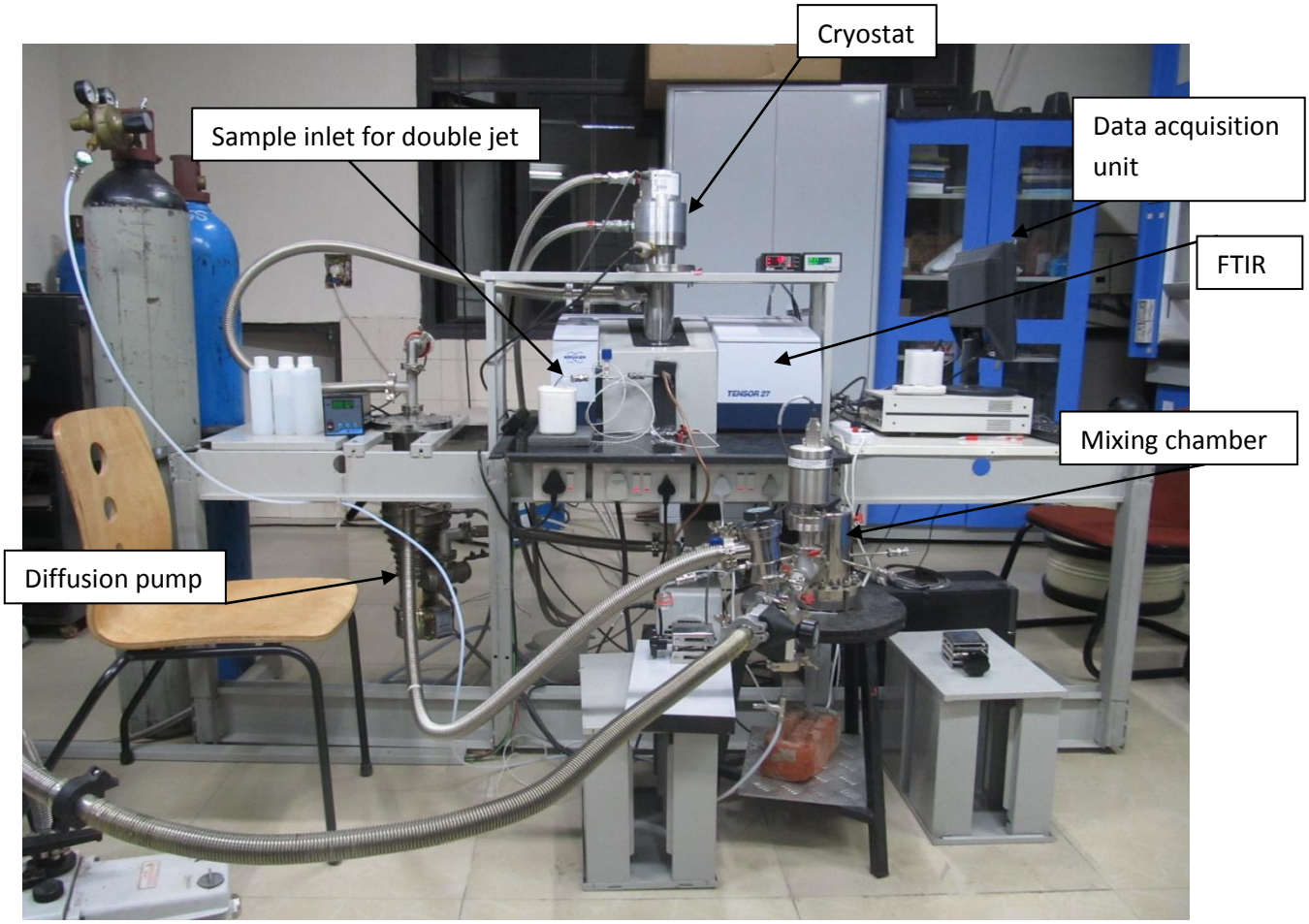

Figure 3: Matrix isolation infrared spectroscopy set-up.

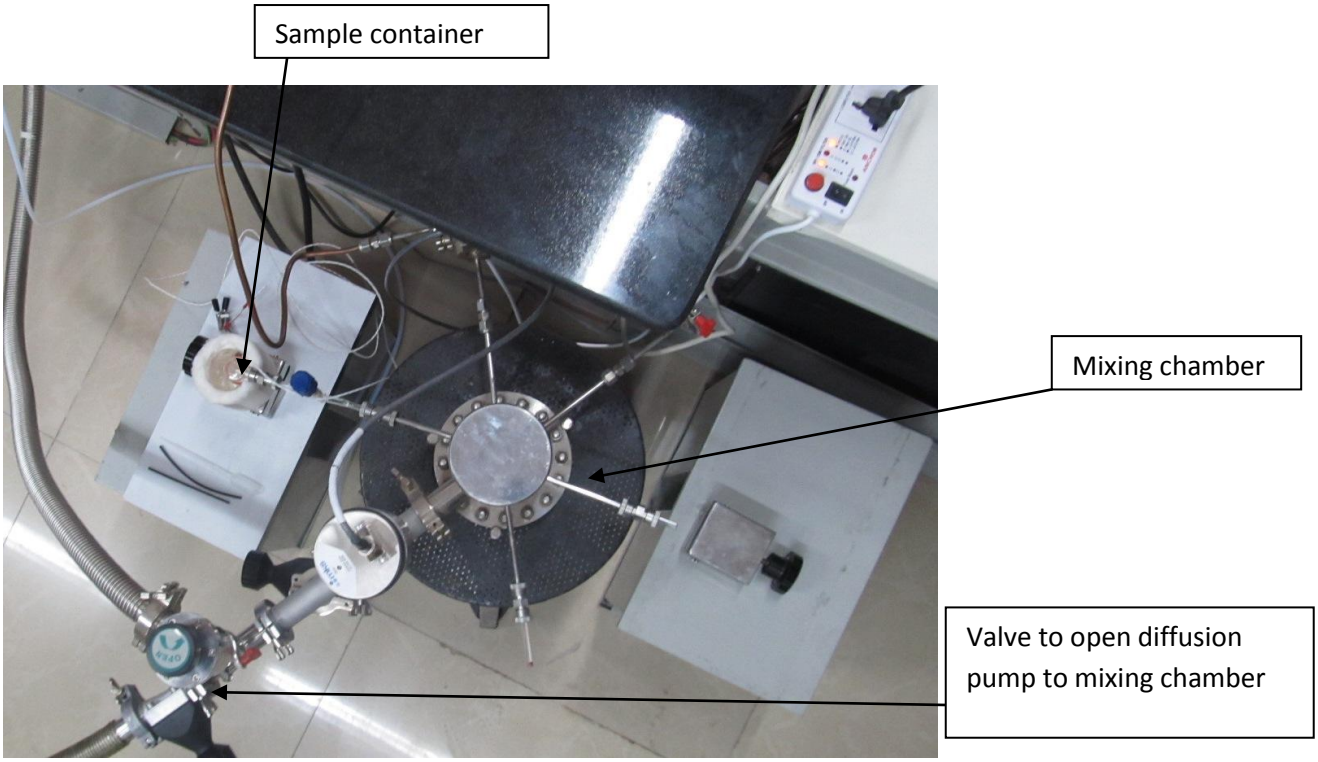

Figure 4: Mixing chamber

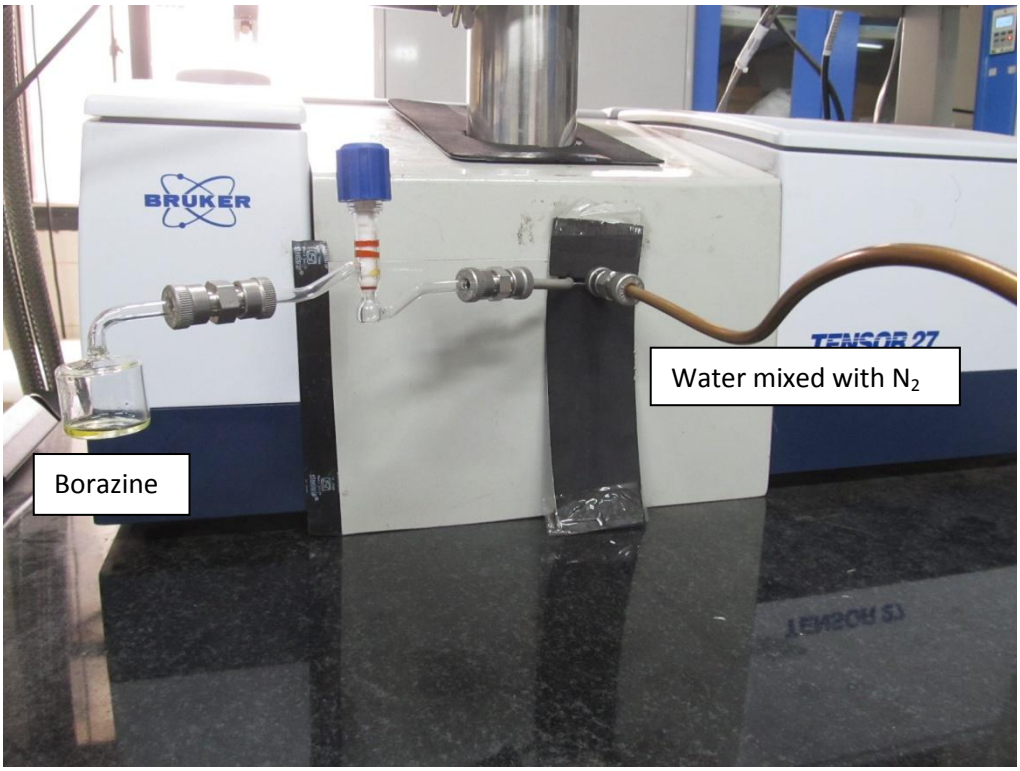

Figure 5: Double jet

CRYOSTAT

The cryogenic temperature is required to solidify the inert gas to form the matrix and also to prevent diffusion of the trapped species. In order to achieve low temperatures as in 77K, 20K, 10K microrefrigerators with nitrogen, hydrogen and helium as working fluids respectively are widely available commercially. The one that was used in this work has a closed cycle helium compressor (Fig. 6). It uses a Sumitomo closed cycle helium compressor (HC-4E1 Helium compressor) for cooling. Expansion of these gases at high pressures cools the surface of the window [26].

The cryostat has the following five main parts [27]

a. Cold head
b. A helium compressor
c. Temperature control unit
d. An optical extension set
e. Trapping surface

The closed cycle cryostat used in our set up works on the Gifford McMahon cycle. The expander, commonly known as the cold head or coldfinger, is where the Gifford-McMahon refrigeration cycle takes pace. It is connected to a compressor through two gas lines for the working fluid (Helium) and an electrical power cable. One of the gas lines supplies high pressure helium gas to the expander, the other gas line returns low pressure helium gas from the expander. The compressor provides the necessary helium gas flow rate. The vacuum shroud surrounds the cold end of the expander in vacuum, limiting the heat load on the expander caused by conduction and convection. The radiation shield is actively cooled by the first stage of the expander and insulates the second stage from the room temperature thermal radiation being emitted from the vacuum shroud. Further, in addition to these major components, the closed cycle cryocooler is often accompanied by several support systems. Typically laboratory systems will have an instrumentation skirt, which provides a vacuum port and electrical feed throughs, as well as a temperature controller to measure and adjust the sample temperature. The system also needs electricity, cold water for the compressor, and a vacuum pump for the sample space.

The first two parts is the basic unit of a closed cycle cryostat. There are two gas lines that are connected from this to the compressor. One provides high pressure helium gas to the

expander. The displacer is driven by this difference in pressure. This causes expansion and hence cooling of the gas at the bottom. The other gas line removes the cold helium gas. This flow removes heat from the system. To control the temperature at and above 12 K, we use a heater that is sensitive to temperature, hence a temperature control unit mounted on the cold window. The window was made of potassium bromide as it is infrared transparent. There are four ports that are around this window. One is made of quartz for viewing and carrying out UV-visible photoradiation experiments. The other is the inlet of deposition gas. The trapping surface can be made of many different materials but that depends upon the spectral region that we have to pass through them and low thermal conductivity.

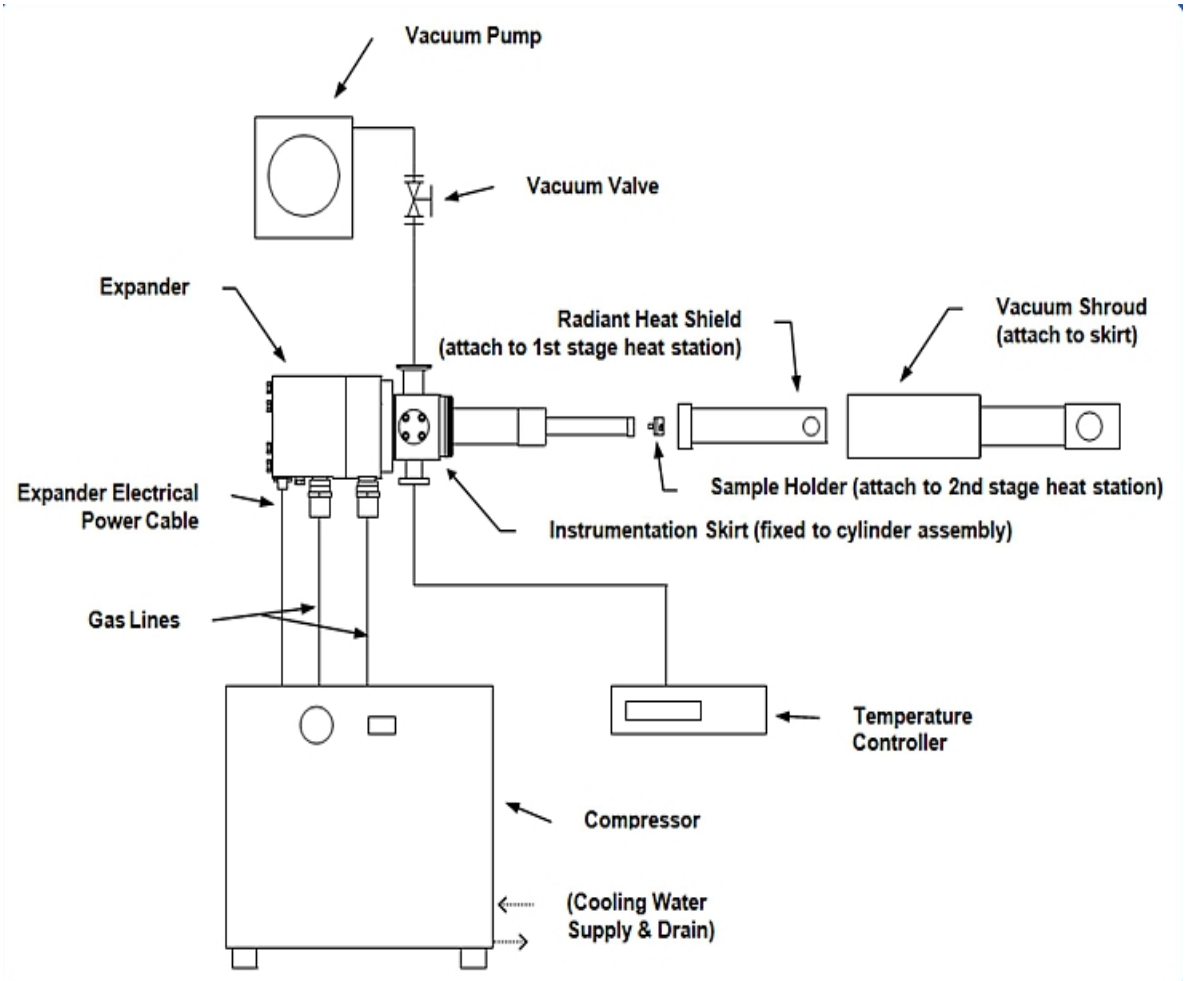

Figure 6: Set up of closed-cycle Helium cryocooler

(Source: www.arscryo.com/TechNotes)

Gifford McMahon Refrigeration Cycle

The refrigeration cycle starts with the rotation of the valve disk opening the high pressure path allowing the high pressure helium gas to pass through the regenerating material into the expansion space. The pressure differential drives the piston "up" allowing the gas at the bottom to expand and cool. The rotation of the valve disk then opens the low pressure path allowing the cold gas to flow through the regenerating material removing heat from the system. Finally the pressure differential returns the displacer to its original position completing the cycle.

Vacuum system

Vacuum pumps are classified based on the chemical or physical phenomenon that is responsible for pumping the gas molecules out of the vacuum vessel. Oil diffusion pump (Edwards, Diffstack MK2 series 100/300) is used to evacuate the cryostat. It has pumping speed of 280 litres per second. This cryostat evacuation system has another rotary pump (Edwards) apart from the diffusion pump. Another rotary pump (Hind Hivac, Model No: ED6) was also used to initially evacuate the vacuum system with a pumping speed of 200 L/m. To isolate the cryostat from the diffusion pump a butterfly valve was used. The vacuum achieved is ~10^{-6} mbar. This is measured using digital penning gauge (DPNG-211). For pressures above 10^{-3} mbar, a Pirani gauge 26 (Edwards APG 100 Active Pirani Gauge) is used.

FTIR spectrometer

The vibrational spectra of the trapped molecules in the matrix were recorded using a Bruker Tensor 27 FTIR spectrometer. The resolution of this instrument is 0.50 cm^{-1}. The working and instrumentation of FTIR can be found in many literatures [28]. Typically 8 scans are taken to obtain good signal-to-noise ratio. All spectra are recorded in the region of 4000 to 400 cm^{-1}. After the sample and matrix were deposited at 12 K, a spectrum of the matrix isolated species was recorded. After recording this deposition spectrum the temperature of the matrix was raised to around 30 K. The matrix was kept at this temperature for about half an hour to one hour using the temperature controller unit (Lakeshore Instruments). The matrix was then again cooled back to 12 K and a spectrum was recorded.

Sample introduction system

The basic requirement for conducting a MI experiment of a desired sample is that the compound should possess a vapour pressure large enough for deposition. For compounds which have a low vapour pressure are heated to a level to deposit them on the cold window whereas for compounds with high vapour pressure are cooled using a slush bath of ethanol and liquid nitrogen and maintained at a particular temperature to get optimum vapour pressure. To start with a mixture of analyte and matrix was prepared in a stainless steel mixing chamber of one liter capacity, which was introduced to the vacuum system through a single effusive nozzle. There are also other sources by which desired samples are introduced in the vacuum system namely- Double jet effusive nozzle and Hot nozzle source. In case where the analyte has low vapour pressure, deposition is carried out using a double jet nozzle system in which through one of the nozzles matrix gas is allowed to effuse out, while the second nozzle is used to introduce the sample into the vacuum system. On the other hand, in order to identify the vibrational features for higher energy structures of the sample deposition was performed through a hot nozzle source, where the nozzle was maintained at various elevated temperatures This entire setup including the sample container and the mixing chamber is kept under vacuum.

Single jet system: Here, the sample is taken in a glass container that is connected to a stainless steel mixing chamber. Then the inert gas is let in and mixed with the sample. After that, using a single jet this mixture is allowed to deposit in the cold window.

Double jet system: Here one sample is taken and allowed to deposit directly without dilution with inert gas before deposition on the window through effusive nozzle. The inert gas which can have the other analyte molecule is deposited using a separate nozzle.

2.4 Procedure

Synthesis

Borazine was prepared using the method described by Jun Sheng Li et. al [29]. 250 g of tetraglyme (Sigma-Aldrich, ≥99%) was taken in 500 mL roundbottomed flask and dried over sodium for a day. The purity was checked by adding some benzophenone to ensure

complete absence of water. 20 g of $NaBH_4$ (Sigma-Aldrich, 98%) was dissolved in tetraglyme. 50 g of $(NH_4)_2SO_4$ (Merck, ≥99%) and 1 g of the the catalyst, $AlCl_3$ (Sigma-Aldrich, 99.99%) was taken in a three-necked round bottomed flask. The entire setup was assembled in a glove box in an inert atmosphere environment, maintained using Ar. A condenser was attached to one neck, addition-funnel to the second neck and the third neck was connected to Schlenk line.

The solution of $NaBH_4$ in tetraglyme was added to the round bottom flask containing ammonium sulphate and the catalyst. The reaction flask was heated in an oil bath to a temperature not exceeding 50 ^{0}C. After the entire solution was added, the reaction mixture was kept at the desired temperature for a further period of about three hours. The entire system was kept under nitrogen atmosphere during the reaction. The scheme of this reaction is shown in figure 7.

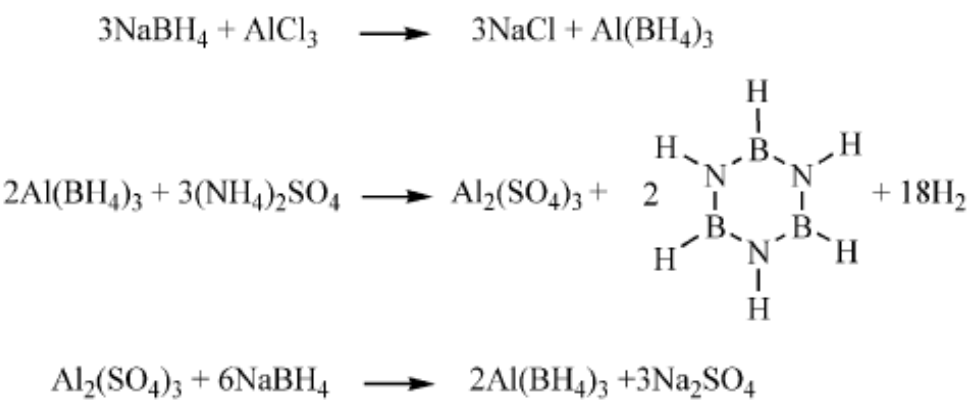

Figure 7: Scheme of the synthesis of borazine

While pure borazine could have been isolated from the tetraglyme by distillation, the extreme reactivity of borazine to moisture precluded such a strategy. Even the water that was desorbed from the glass container was sufficient to decompose the borazine. Hence the borazine that was prepared was retained in the tetraglyme solvent and was used as such. The vapour pressure of tetraglyme being extremely low relative to that of borazine, the vapour phase over the borazine-teraglyme system solely consisted of borazine which was used in preparing matrix isolated borazine. Borazine in tetraglyme was stable as it did not get into contact with water and hence could be used without concern of it decomposing. As abundant caution, the borazine in tetraglyme was stored inside an argon atmosphere glove box. The characterization of borazine was done by using Ar gas as matrix in the MIIR experiment and

the results were compared to a previously reported MIIR experiment of borazine by Kaldor and Porter [30].

Double jet experiments

As stated previously, Borazine being highly moisture sensitive, it could react with water in vapour phase. This was primarily the reason for using a double jet where water and borazine were let in through separate nozzles. Water was mixed with the inert gas in the mixing chamber, but the other sample (borazine) was connected to an inlet or a jet directly opening on to the window kept at 12 K. Both jets were opened at the same time. Deposition of both the samples took place simultaneously.

Chapter3

Computational Procedure

Computational calculations were performed using Gaussian 09 package [31]. Molecular properties such as structures, energies and frequencies were calculated to corroborate our experimental results.

There are many *ab-initio* methods available for doing the computational calculations. Some of the popular methods are: Hartree-Fock methods (HF), Density Functional Theorem (DFT), Møller–Plesset perturbation theory (MPn) (where n denotes the order of perturbation), Configuration interaction (CI), Coupled cluster (CC), Multi-configurational self-consistent etc.

In DFT methods, all electronic properties of system to be determined from the electron density is a function of just three variables (x, y, z). One of such functionals is BLYP (Becke-Lee-Yang-Parr) which includes some HF exchange. It involves both electron spin densities and their gradients. There are also hybrid functionals which define the exchange functionals as a linear combination of HF, local and gradient-corrected exchange terms. The most commonly used functional is B3LYP. The B3LYP method uses the Becke three-parameter non-local exchange functional [32, 33] with non-local correlation of Lee et. al [34]. Unlike HF, DFT includes electron correlation and hence more accurate. Recently, advance modifications in DFT functionals have been introduced, named as Minnesota functionals (M06). It has been designed by employing some strategies. These are 1) constraint satisfaction, 2) modelling the exchange correlation hole, 3) mixing Hartree-Fock and approximate DFT exchange. The M06 suites of functionals are set of four meta-hybrid GGA DFT functionals (generalized gradient approximation (GGA) in which the density functional depends on the up and down spin densities and their reduced gradient). These M06 functionals are considered good for the dispersion interactions. In M06-2x, 2x refers to the percentage of HF exchange which is 54% in this case [35].

Møller–Plesset perturbation theory is one of the several quantum chemistry post-Hartree Fock-*ab initio* methods in the field of computational chemistry which was developed

in 1934 by Christian Moller and Milton S. Plesset [36]. It improves on the HF method by adding electron correlation effect by means of Rayleigh-Schrondinger perturbation theory to second (MP2), third (MP3) and fourth order (MP4). In this theory, there is an unperturbed Hamiltonian operator, and a small perturbation (often external) is added to it. Systematic studies of MP perturbation theory have shown that it is not necessarily a convergent theory at high orders.

Geometry optimization of complexes were done at MP2 and M06-2x levels of theory. Vibrational frequency mode analysis were done at MP2, M06-2x and B3LYP levels of theory. The basis set used was 6-311++G(d,p) for these calculations. The vibrational computations were done to confirm that the structures obtained correspond to minimum on the potential energy surface. The computed vibrational frequencies were scaled, by comparing the computed frequencies of borazine, with the observed experimental frequencies, in a given matrix. These scaling factors were then used to compute the frequencies in the complex.

Zero point vibrational energies were also obtained from the frequency calculations which was used to calculate the ZPE corrected energies for the various complexes.

Stabilization Energies for various complexes:

The stabilization energy of a complex is given by:

$$E = E_{AB} - (E_A + E_B)$$

where, E_A, E_B and E_{AB} represent the energies for the monomers A, B and complex AB respectively. Negative value of E signifies that the complex is more stable relative to the precursors. The stabilization energy of the complex corrected for zero point energy (ZPE) was also calculated. When the energy of complex (E_{AB}) is computed, the basis functions used are those of both the monomer subunits. Whereas, for computing the energy of the individual precursors (i.e. E_A and E_B), the basis functions only corresponds to the precursors used. As the number of basic functions becomes larger in the computation of the complex, the energy obtained will be lower, due to the fact that each monomer can now use the basic functions of other. Stabilization energies thus derived from the calculated energies E_A, E_B and E_{AB} will be

overestimated and the error is referred to as the basis set superposition error (BSSE). The best way to eliminate the BSSE is to increase the basis set until the stabilization energy is the desired minimum with the tradeoffs of large computation times for even small systems. The commonly used method to correct for BSSE is through the use of the counterpoise correction method proposed by Boys and Bernadi [32]. In this scheme, all the energies of monomer E_A, E_B and the complex E_{AB}, are computed in the same basis set spanned by the functions of the complex AB.

The stabilization energies are then obtained as follows.

$$E = E_{AB}(AB) - \{E_A(AB) + E_B(AB)\}$$

where, $E_A(AB)$ = Energy of the monomer A using the basis set AB
$E_B(AB)$ = Energy of the monomer B using the basis set AB
$E_{AB}(AB)$ = Energy of the complex AB using the basis set AB

Zero point energy correction (ZPE correction)

ZPE is the energy that a molecule possesses even at absolute zero temperature. Stabilization energies to be experimentally meaningful must be corrected for the ZPE, as follows:

$$\mathbf{E_{total} = E_{cal} + ZPE}$$

Atoms- in-molecules (AIM):

This theory was first proposed by Richard Bader which is based on electron density topology [33-35]. According to AIM, the molecular structure is revealed by the stationary points of the electron density together with the gradient paths of the electron density that originate and terminate at these points. The development of AIM was based on the assumption that, since the concepts of atoms and bonds have been and continue to be so useful in interpreting, classifying and predicting and communicating chemistry, they should have a well defined basis.

For performing the (AIM) analysis the wave functions corresponding to the optimized geometry of a molecule or complex are generated using the Gaussian package. From the

electron density plot one can obtain the bond critical points, charge density ρ, Laplacian of charge density $\nabla^2\rho$, which is also the trace of the Hessian of ρ. The charge density, ρ(r), is a physical quantity which has a definite value at each point in space. Each topological feature of ρ(r), where it is a maximum, a minimum, or a saddle point, is associated with a space called a critical point, where the first derivative of ρ(r) vanishes. The sign of the second derivative at this point determine whether the function is maximum or minimum.

The critical point (CP) is labeled by giving the values (ω, σ). For example, (3, -1) critical point means, three non-zero curvatures and one positive and two negative eigenvalues.

(3, -1) CP corresponds to a bond between two atoms, a (3, +1) CP to a ring, a (3, +3) CP to a cage and a (3, -3) CP corresponds to a maximum. The numbers of critical points of all types, which can coexist in a system with a finite number of nuclei, are governed by the Poincare-Hopf relationship.

$$n - b + r - c = 1$$

where, n is the number of nuclei, b is the number of bond critical points, r is the number of ring critical points and c is the number of cage critical points.

The sum of three Hessians (λ1, λ2, λ3) at a bond critical point, the quantity $\nabla^2\rho$, provides a useful characterization of the manner in which the electronic charge density is distributed in the inter nuclear region. If the value of charge density ρ ($<10^{-1}$ au) and the curvature of charge density are large, Laplacian of charge density may be positive or negative usually in the same order of magnitude as ρ then the interaction is of shared type, typical of covalent interaction. For the closed shell interactions, such as hydrogen bond complexes, Van der Waals complexes and ionic systems, the charge density ρ ($\sim10^{-2}$to 10^{-3} au) at the bond critical point is quite small and the Laplacian of the charge density is positive.

Chapter-4

Results and Discussion

4.1 Experimental Details

Figure 8 (a,b) shows the spectrum of matrix isolated borazine. Intense multiplet absorption is observed at around 3477.1 and 3470.8 cm^{-1}, latter being the more intense feature, which corresponds to the N-H stretch of borazine. The features are probably split due to site effects. A peak with multiplet structure was observed at 2587.5 and 2512.1 cm^{-1}, with the latter being the more intense feature, which correspond to the B-H stretching modes. The multiplet structure in this vibrational feature is due to the different isotopomers discussed earlier. Another multiplet was also observed at 1460.3 cm^{-1} (Fig. 8(c,d)) which correspond to bending modes involving boron. The computed spectrum in figure 8 is scaled using the experimental N-H stretch at 3470.8 cm^{-1}. The good agreement between the computed and the experimental frequencies confirms the assignments for the various modes of borazine.

The spectral features of water (Fig. 9) obtained in this experiment are in good agreement with reported values in literature [36]. In the spectrum of matrix isolated water, the peaks at 3727 and 3634 cm^{-1} corresponding to the antisymmetric and symmetric stretch of O-H. The small feature at 3715 cm^{-1} is due to the formation of the H_2O dimer.

When borazine and water were codeposited, and the matrix then annealed, new product features were observed at 3394.0, 3401.5 and 3483.3 cm^{-1} in the region of the N-H stretch of borazine as shown in figure 9. In the region of the O-H antisymmetric stretch of water, a product band was observed at 3720.6 cm^{-1}. That these were features due to the borazine-water adducts, was confirmed by the fact that these features increased in intensity when the concentration of either of the two precursors, borazine or water, was increased. It must be noted, that the product features were observed even when no water was deliberately introduced, as water is present as a ubiquitous impurity. However, the observation that the intensity of the product features depended on the concentration of both borazine and water confirms their origin (Fig. 10). Experiments were performed at two different matrix:water

ratios of 3:1000 and 6:1000. Since borazine was taken in tetraglyme in which its concentration was not estimated, it was not possible to determine the exact the matrix to sample ratios for borazine. However, since its variation of vapour pressure with temperature was known, it was possibile to estimate the relative changes in the borazine concentration in the matrix in the various experiments performed, which are shown in figure 10.

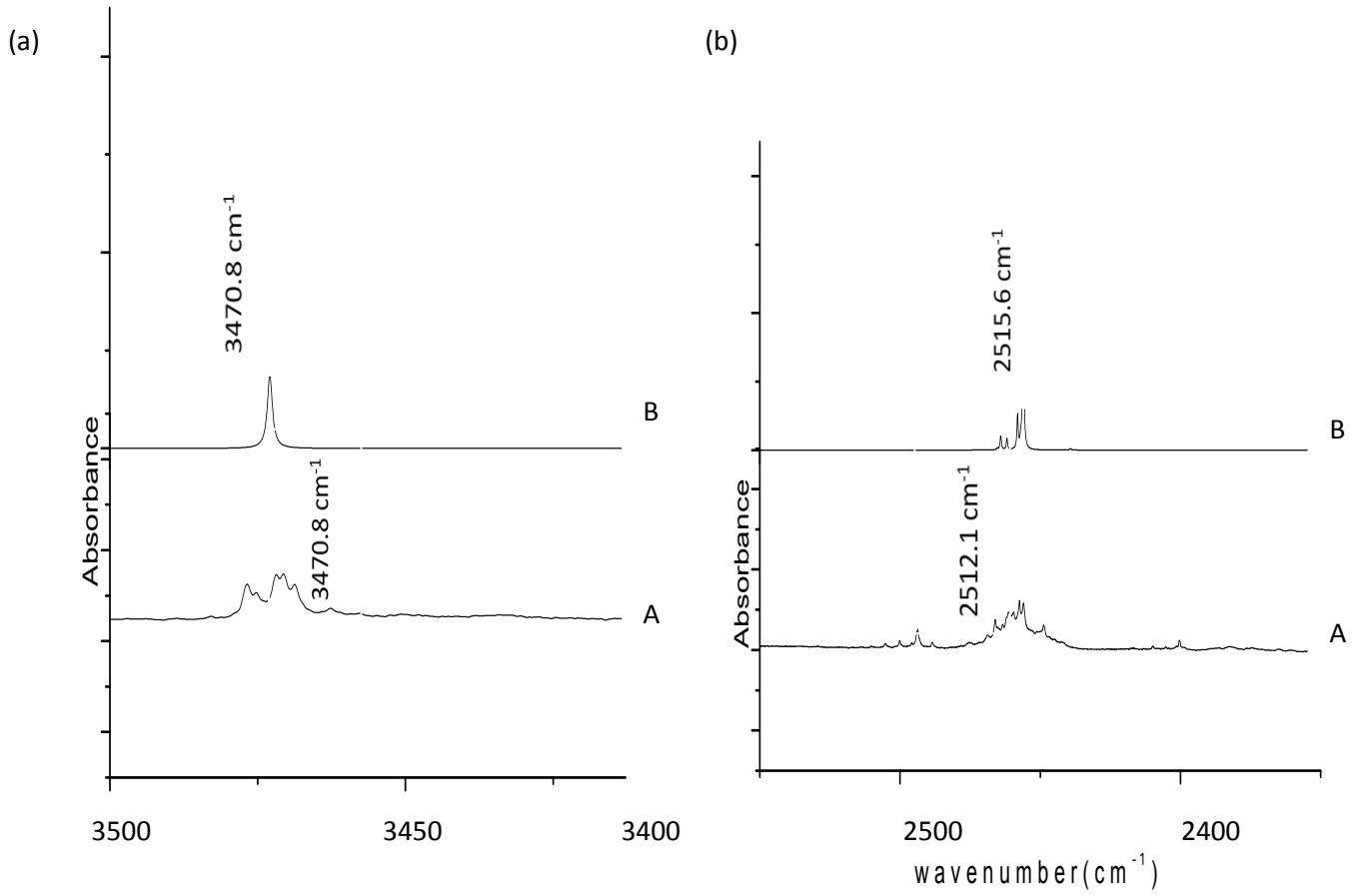

Figure 8 (a, b): (A) Matrix isolated infrared spectrum of borazine trapped in a nitrogen matrix, (B) Computed spectrum at the MP2/6-311++G(d,p). Grids show the spectra in the following ranges (a) 3500 cm^{-1} - 3400 cm^{-1}, (b) 2700 cm^{-1} - 2300 cm^{-1}.

(c) (d)

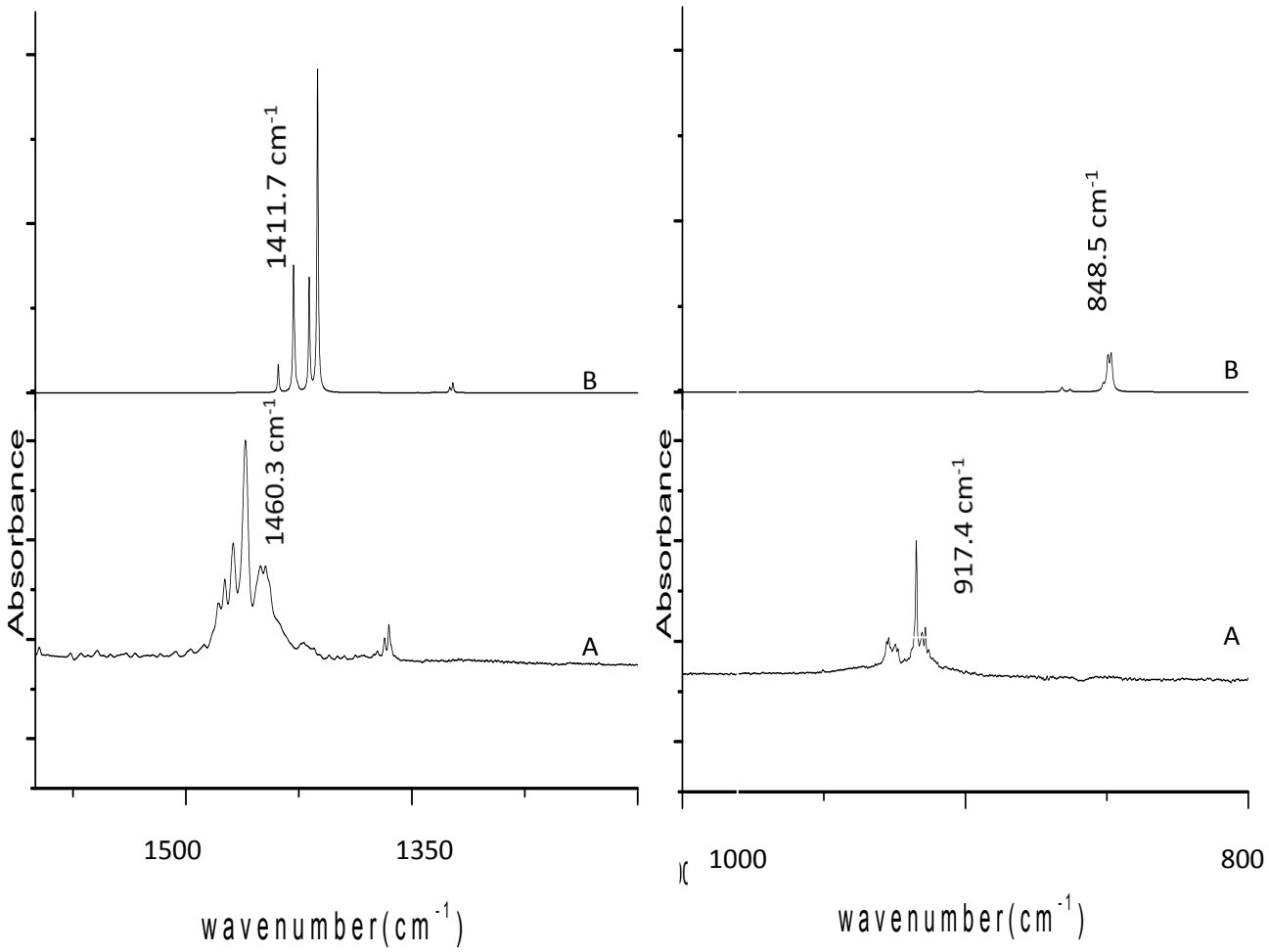

Figure 8 (c, d): (A) Matrix isolated infrared spectrum of borazine trapped in a nitrogen matrix, (B) Computed spectrum at the MP2/6-311++G(d,p). Grids show the spectra in the following ranges (c) 1600 cm^{-1} - 1200 cm^{-1}, (d) 1000 cm^{-1} – 800 cm^{-1}.

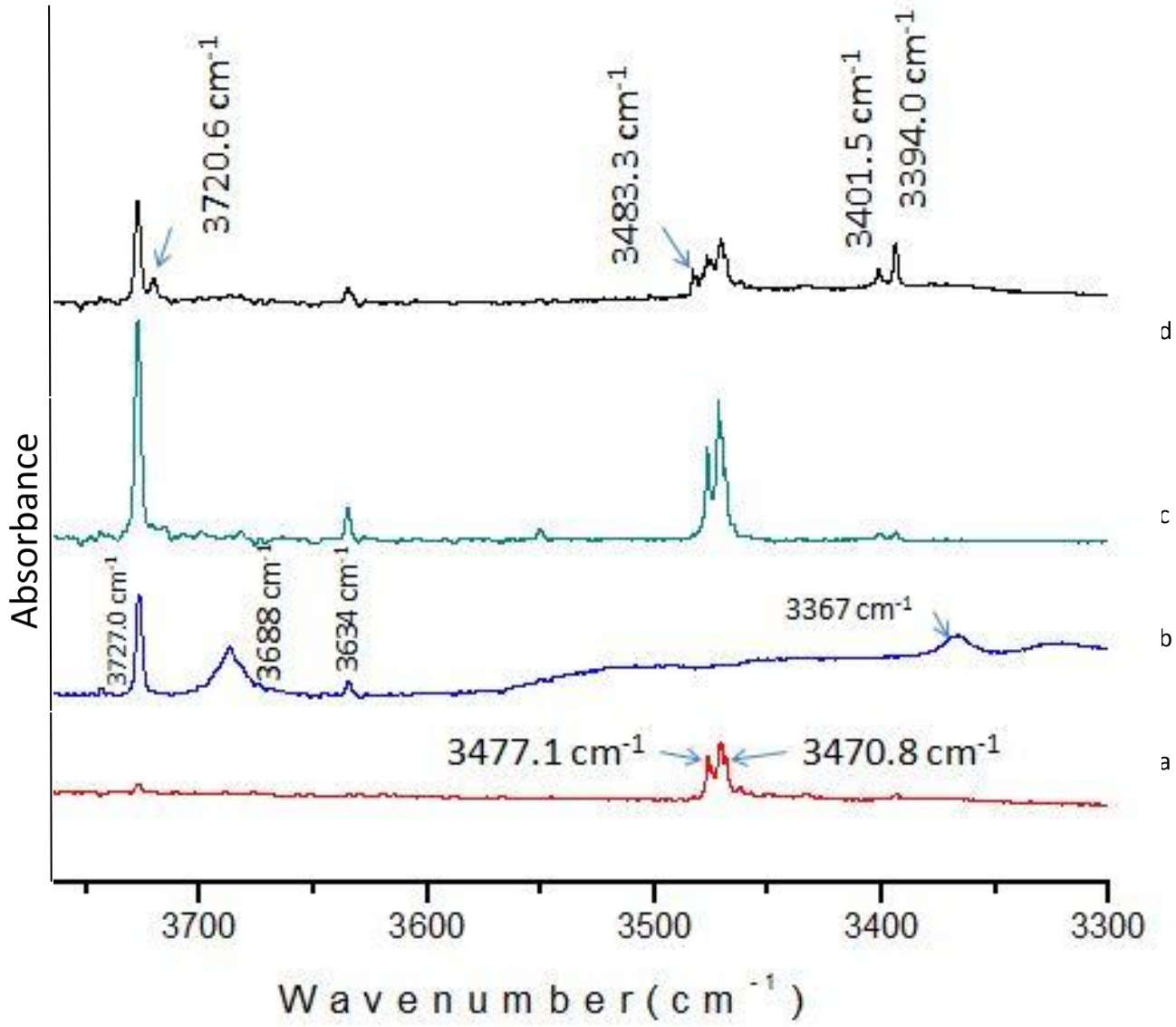

Figure 9: Spectrum of (a) borazine, (b) water, (c) borazine and water co-deposited at 12K, (d) Sample in 'c' annealed at 30 K.

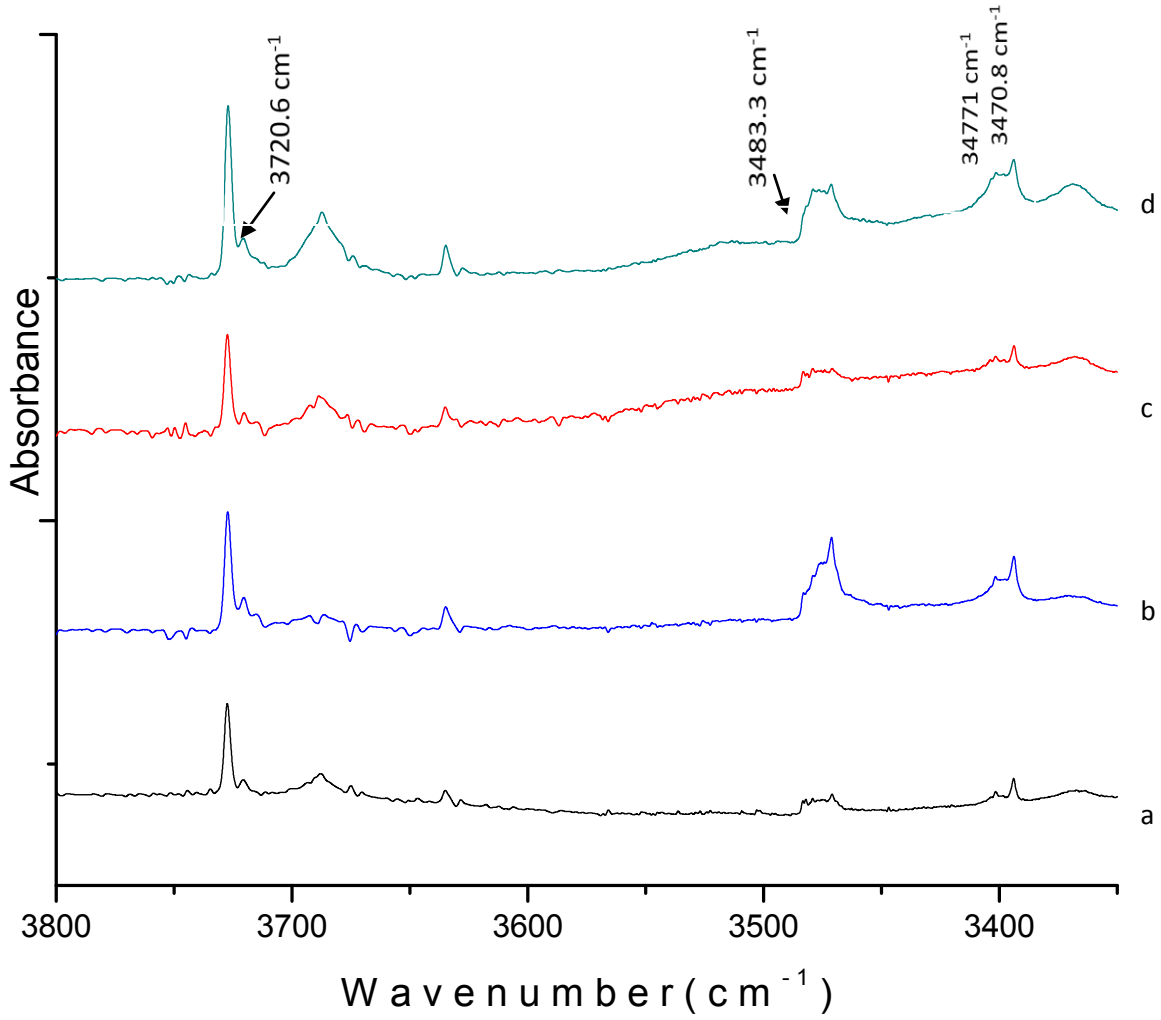

Figure 10: Spectra showing the concentration dependence for the borazine-water complex. (a) x:3 mBar:1270 mBar (b) x:6 mBar:1270 mBar (c) 4x:3 mBar:1270 (d) 4x:6:1270 mBar.

4.2 Computational Details

The computational calculations were performed using Gaussian-09 program suite. The optimized energy were calculated at B3LYP, M06-2x and MP2 levels of theory. Stabilization energies were computed and also individually corrected for the zero point energy (ZPE) and the basis set superposition errors (BSSE). BSSE correction was implemented using the counterpoise (CP) scheme of Boys and Bernadi [32]. The frequency calculations were performed at M06 and MP2 level of theories mentioned above to ensure that the optimized geometries were indeed a minimum on the potential surface and also to aid us in assigning the features observed in the experiments. Using the computed experimental frequencies, the infrared spectrum of the complexes and the monomers were also simulated using Synspec assuming a linewidth of 0.1 cm^{-1}. Atoms in Molecule theory was performed at M06-2x and MP2 to identify the critical points in the complexes to understand the bonding features. 6-311++G(d,p) basis set was used in all calculations. A similar work has been done before of the interaction between borazine and first-row hydrides [37, 38].

Our computations at the MP2 and M06-2x levels indicated three complexes for the borazine-water system. All three complexes yielded all real frequencies, thus confirming them to be minima on the potential surface. The stabilization energies of these complexes are given alongside each structure in figure 11. Table 1 gives the stabilization energies of these complexes at various levels of theory. While the actual values of the stabilization energies were different at the various levels of theory employed, the relative energy ordering of the complexes were the same at all levels of theory.

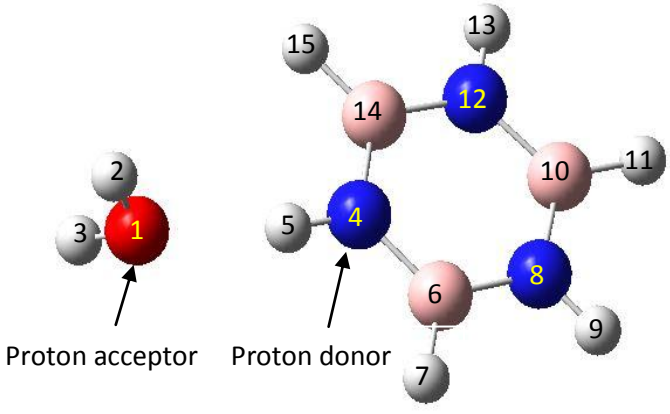

Complex 1

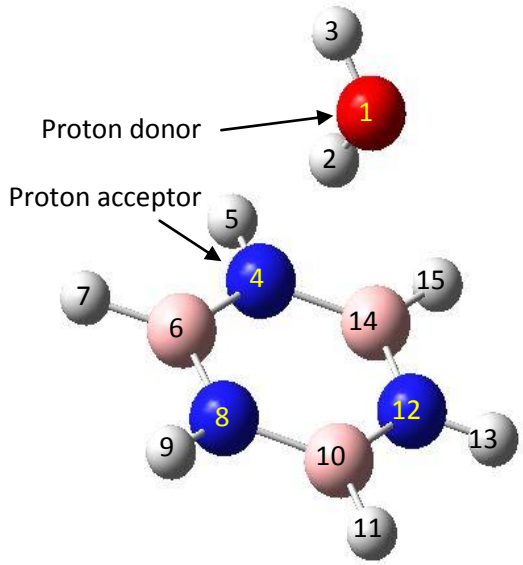

Complex 2

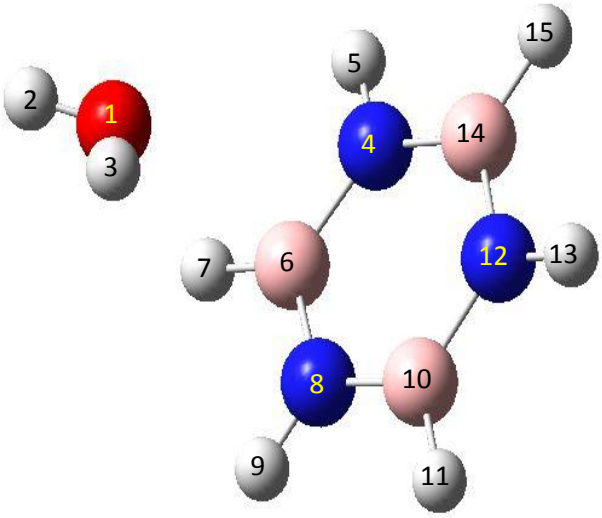

Complex 3

Figure 11: Structure of the borazine-water complexes calculated at MP2/6-311++G(d,p)

The global minimum corresponded to a structure in which borazine was the proton donor through the N-H moiety to the water (Complex 1). In fact this structure was the global minimum at all levels of theory that we explored. At the MP2/6-311++G(d,p) level, the N-H..O hydrogen bond distance in this complex is 2.066 Å. The next higher energy complex was complex 2, where water served as the proton donor to the nitrogen of borazine. In this

complex, the O-H..N hydrogen bond distance was computed to be 2.426 Å. Located further above, was another local minimum (complex 3), in which the oxygen of water was weakly bonded to the boron in borazine, which can be considered to be the boron analogue of the hydrogen bond, the "boron bond". The B..O distance in this complex was computed to be 2.955 Å.

Table 1: Raw/ZPE corrected/BSSE corrected interaction energies (kcal/mol) for complexes 1, 2 and 3 at B3LYP, M06-2x and MP2 levels of theory at 6-311++G(d,p).

	B3LYP	**M06-2x**	**MP2**
Complex 1	-3.611/-2.493/-3.073	-4.334/-2.813/-3.534	-4.704/-3.482/-2.947
Complex 2	-1.714/-0.722/-1.354	-3.828/-2.645/-3.099	-2.701/-1.689/-1.318
Complex 3	Minima not located	-1.443/-0.743/-0.598	-1.596/-0.710/0.130

4.3 Vibrational assignments

The experimentally observed product bands in the borazine-water codeposition experiments were assigned based on the computed values obtained at MP2/6-311++G(d,p). As explained before, the computed frequencies for the complexes, were scaled using scaling factors that were computed by comparing the computed and experimental features of the monomer precursors. The frequency mode assignments are given in table 2. The computed and experimental spectra of the complexes are shown in figure 12.

4.2.1 N-H stretch in borazine

Figure 8 shows the spectrum of borazine, with a strong absorption at 3470.8 and 3477.1 cm^{-1} that corresponds to the N-H stretch of borazine. These were further split into multiplets. These multiplets arose due to site effects. This assignment is corroborated by our computations. The doublet at 3394.0 and 3401.5 cm^{-1} were due to the borazine-water complex, are assigned to the N-H stretch of complex 1, which agrees well with the computed scaled frequency of 3408.5 cm^{-1}. The features of the complex occur as doublets probably due to site effects. The N-H vibration in the complex is therefore red shift by ~76.8 cm^{-1} from N-

H mode in uncomplexed borazine. This shift is typically of N-H..O interactions. Shifts in similar systems were seen in the work done by H. M. Muchall et.al. [39]

In addition to the features mentioned above, we also observed a feature shifted to the blue of the N-H stretch in free borazine, This features at 3483.3 and 3482.0 cm^{-1} were confirmed to be due to a complex, through its dependence on the concentration of the precursors. Interestingly, this blue shifted N-H feature, was computed to occur due to both complex 1, computed to occur at 3470.2 cm^{-1} and complex 3, computed to occur at 3469.7 cm^{-1}. It may be recalled that complex 3 involved a B..O interaction. Since complex 1 has already been observed, it is tempting to assign this blue shifted N-H feature to this complex. However, the possibility of the formation of complex 3 is not ruled out. Should the feature belong to complex 3, which will be confirmed through more experiments, it would present evidence for the boron bond in the borazine water complex. This N-H stretch frequency shows a not so common blue shift of 12.5/11.2 cm^{-1} from the uncomplexed N-H stretch feature in uncomplexed borazine. Similar non-covalent interactions have been reported where hydrogen does not take part like Cl…O bond and Li bond [40, 41]. These complexes have been observed in MIIR experiments.

4.2.2 O-H stretch in water

We also looked for perturbations in the water submolecule. Figure 10, shows the spectra in the region of the O-H stretch in water. As mentioned above, a product feature was observed at 3720.6 cm^{-1}, which is red shifted by 7.1 cm^{-1} from the antisymmetric O-H stretch in uncomplexed water at 3727.0 cm^{-1}. The O-H stretch in complex 1 was computed to occur at 3716.4 cm^{-1} which therefore can be seen to be in good agreement with the experimental observation; thus providing strong evidence for the occurance of complex 1 in the matrix. The feature due to water in complex 3 is computed to occur near 3703.9 cm^{-1}, evidence for which was not observed in the matrix. This maybe because the feature lies around water multimers.

The features at 2588 and 2515 cm^{-1} in borazine show multiplets due to isotopomers and hence is assigned to modes involving the boron atoms. However, these modes do not show any clear perturbations due to complex formation.

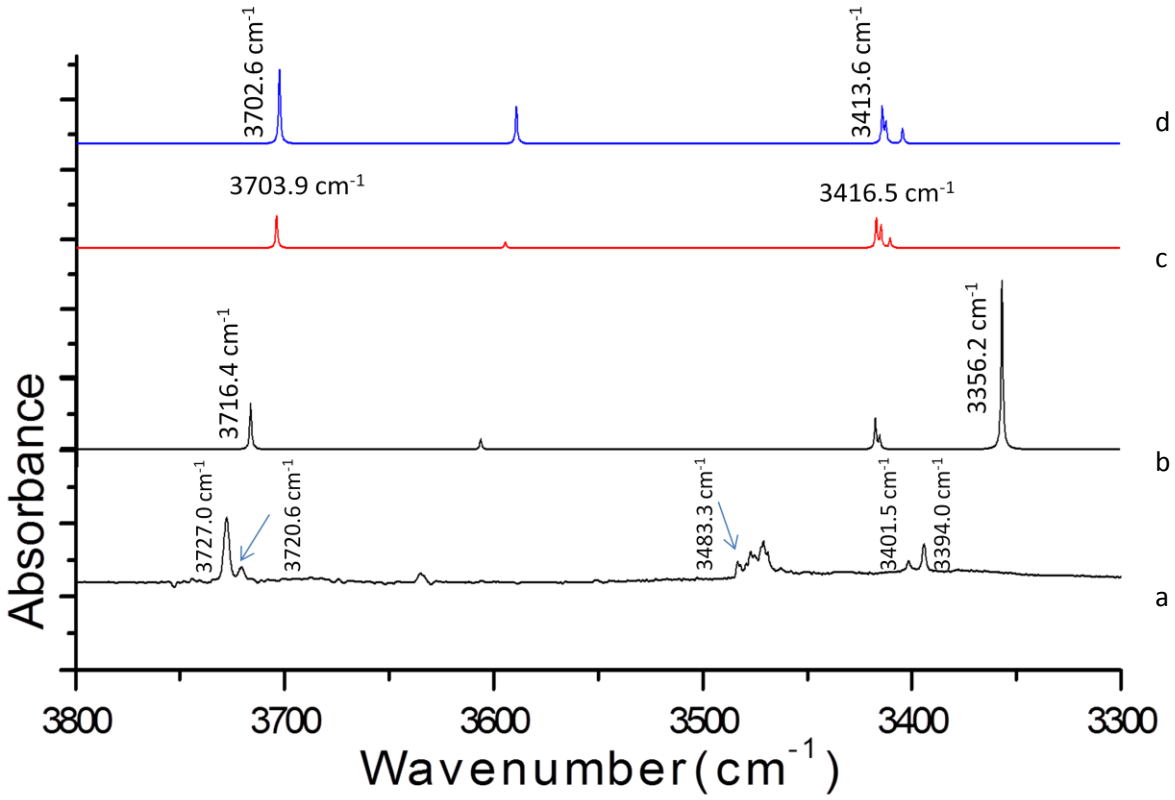

Figure 12: Spectra comparing the computed spectra (MP2/6-311++G(d,p) for each of the complexes with spectra recorded after annealing the matrix at 30K, over the region 3800-3300 cm-1, corresponding to the N-H stretch region of borazine and O-H stretch of water. Experimental spectrum (a) borazine and water codeposited (b) computed spectrum of complex 1, (c) computed spectrum of complex 3 (boron bonded complex), (d) computed spectrum of complex 2 (not observed experimentally).

Table 2: Mode assignments of the submolecules and complexes with scaling factors at MP2/6-311++G(d,p) basis set. The difference between experimental monomer and scaled frequencies of the complexes are given in parenthesis under the respective scaled frequencies.

MP2					
Borazine			Water		
Comp	S F	Expt	Comp	S F	Expt
3670.4	0.9456	3470.8	4003.4	0.9311	3727.0

MP2							
Complex1		Complex2		Complex3		Expt	Mode
Comp	Scaled	Comp	Scaled	Comp	Scaled		
3604.6	3408.5 (62.3)	3666.2	3466.8 (4)	3669.3	3469.7 (1.1)	3394.0 (76.8)	N-H stretch in cmplx 1
3669.8	3470.2 (0.6)	3666.2	3466.8 (4)	3669.3	3469.7 (1.1)	3483.3 (-12.5)	N-H stretch in cmplx 1
3991.4	3716.0 (11.0)	3976.5	3702.1 (24.9)	3978.0	3703.9 (23.5)	3720.6 (6.4)	Water asym stretch in cmplx 1

Comp: computed, Expt: experimental, S F: scaling factor, cmplx: complex, asym: asymmetric

4.4 AIM analysis

To examine the nature of interaction in borazine-water complexes, we used the theory of atoms in molecules (AIM). Using the optimized geometry of the complexes computed at MP2 and M06-2x, we searched for a (3,-1) bond critical point (BCP) shown in figure 13 and figure 14 respectively. The electron density and Laplacian of the electron density (defined as the sum of the Hessian eigenvalues) were analysed at the bond critical point. Table 3 gives electron density and laplacian of electron density at MP2/6-311++G(d,p). Complex 3 is not optimized in AIM at this level of theory. Table 4 gives electron density and laplacian of electron density at M06-2x/6-311++G(d,p). Here all three complexes were optimized where complex 2 is showing a bidentate bond formation and complex 3 is showing a curve bond path.

(a) Complex 1

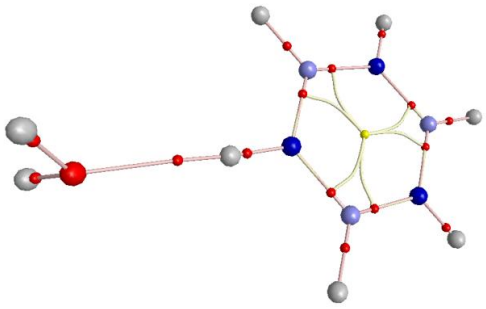

(b) Complex 2

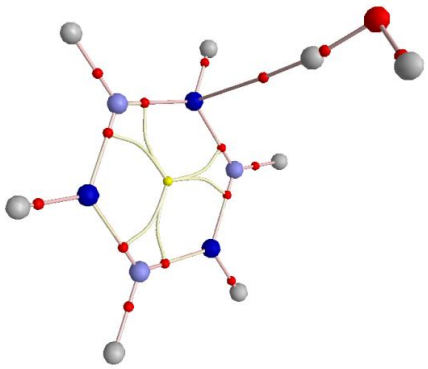

(c) Complex 3

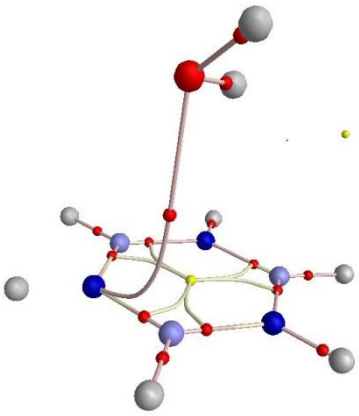

Figure 13: **AIM analysis showing (3,-1) bond critical point (BCP) and (3,+1) ring critical point (RCP) in the complexes at MP2/6-311++G(d,p)**

Table 3: AIM analysis of complexes at MP2/6-311++G(d,p) showing the charge density and Laplacian of charge density at the bond critical point of the interaction between the submolecules.

Complex	$\rho(r_c)$	$\nabla^2\rho(r_c)$
Complex 1	0.0184	-0.01770
Complex 2	0.01106	-0.00824
Complex 3	0.00699	-0.00581

(a) Complex 1

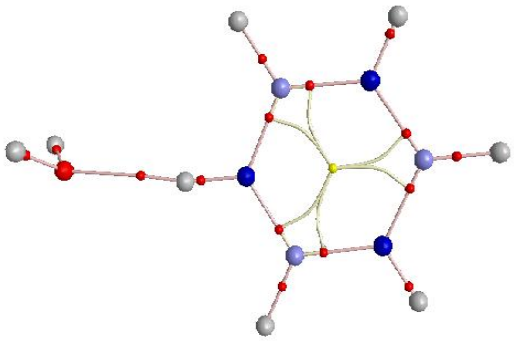

(b) Complex 2

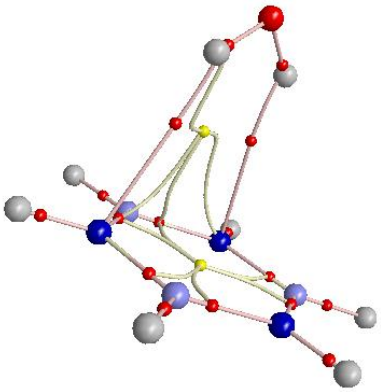

(c) Complex 3

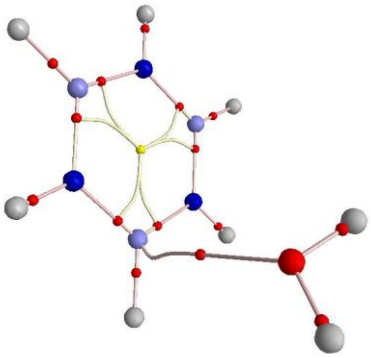

Figure 14: AIM analysis showing (3,-1) bond critical point (BCP) and (3,+1) ring critical point (RCP) in the complexes at M06-2X/6-311++G(d,p)

Table 4: AIM analysis of complexes at M06-2x/6-311++G(d,p) showing the charge density and Laplacian of charge density at the bond critical point of the interaction between the submolecules

Complex	$\rho(r_c)$	$\nabla^2\rho(r_c)$
Complex 1	0.01851	-0.01872
Complex 2	0.00988	-0.00742
Complex 3	0.00813	-0.00698

4.5 Geometrical Parameters

The geometric parameters at MP2/6-311++G(d,p) level are shown in Table 5.

Table 5: Geometric parameters of the monomers and complexes at MP2/6-311++G(d,p).

Parameter	Borazine	Water	Complex 1	Complex 2	Complex 3
N4-H5	1.010 Å	-	1.014 Å	1.011 Å	1.010 Å
N8-H9	1.010 Å	-	-	-	1.010 Å
N12-H13	-	-	-	-	1.010 Å
B14-H15	1.193 Å	-	1.195 Å	1.192 Å	-
B6-H7	-	-	1.194 Å	1.193 Å	1.193 Å
B10-H11	-	-	1.194 Å	1.192 Å	-
O1-H2	-	0.959 Å	0.961 Å	0.962 Å	0.961 Å
O1-H3	-	-	0.961 Å	-	0.962 Å
O1-H5	-	-	2.066 Å	-	-
N4-H2	-	-	-	2.426 Å	-
O1-B6	-	-	-	-	2.955 Å
H5-O1-H2	-	-	121.63°	-	-
H5-O1-H3	-	-	121.71°	-	-
N4-H5-O1	-	-	177.42°	-	-
N4-H2-O1	-	-	-	173.72°	-
B6-O1-H2	-	-	-	-	130.25°
B6-O1-H3	-	-	-	-	104.49°

4.6 Comparison of the borazine-water complex with the benzene-water complex

Matrix isolation studies on benzene-water [42] in Argon matrix indicate that the water molecule is hydrogen bonded to the flat side of the benzene ring i.e there is only global minimum seen in this case. But in the borazine-water complexes, we are able to observe two local minima and one global minimum (i.e. where N-H of borazine interacts with O of water). Complex 2 of borazine-water interaction is analogous to this H-pi interaction of benzene with water, but interestingly, complex 2 was the only borazine-water complex that was not observed experimentally. Further, the concentrations used for benzene are 1:140 and 1:1200 and for water it is between 1:150 and 1:300. In our paper, we have given the temperature dependence of the concentration of the complexes. There was a red shift in the frequencies observed in the stretching region and a blue shift in the bending region, as expected.

In the paper by H. S. Gutowsky et.al. [43], the distance between centre of mass of benzene and water is 3.329 Å. The potential is a sixfold barrier with a shallow minima allowing water to freely rotate with its axis of rotation being same as the inertial frame as the potential constraints it. Even deuterated water shows similar interaction.

At MP2/6-311++G(d,p) benzene-water has a stabilization energy of –4.514 kCal mol^{-1} whereas complex at the same level of calculation has a stabilization energy of –2.701 kCal mol^{-1}. This comparison shows us that the interaction of water with benzene and interaction of water with borazine are very different.

Chapter 5

Conclusion

This thesis provides a computational and experimental study of interactions between borazine and water. The motivation of the present work was to study the complexes of borazine and water and compare them with those of the benzene-water system, benzene being the organic chemistry analogue of borazine. It has already been established that the benzene-water system manifests an H-π interaction. The computations on the borazine-water system were performed using the GAUSSIAN 09 suit of programs. The computations, which involved, arriving at the optimized structures, calculations of the stabilization energies of the complexes and vibrational frequencies were carried out at B3LYP, M06 and MP2 levels of theory using 6-311++G(d,p) as the basis set. AIM calculations were also done to determine the nature of bonding in these complexes by examining the bond critical point for the complexes. Three complexes were obtained computationally out of which one was clearly observed in the matrix, which involved an N-H..O interaction. In this complex, complex 1, the borazine was the proton donor through its N-H group and water was the proton acceptor. This complex was also indicated to represent the global minima on the borazine-water potential surface. At this time, it is not clear if we were also observing complex 3, which showed an interesting B..O interaction. This bond, which we refer to as the boron bond, was indicated to be a local minima and to manifest a blue shifted N-H stretch. More work will be required to establish the presence of this complex in the matrix. Complex 2, was a structure in which O-H of water served as a proton donor and N of borazine is the proton acceptor. This complex was the closest in structure to the H-π interaction in benzene-water system. However, no evidence was found for the formation of this complex. It is therefore clear that the borazine-water system has little in common to the benzene-water system.

This work clearly indicates that the boron containing systems have surprises to show in the study of the hydrogen bonding systems. Exploring the hydrogen bonded interactions in such systems is therefore an area of work that clearly begs to be performed.

References

1) P. J. Fazen, E. E. Remsen, J. S. Beck, P. J. Carroll, A. R. McGhie, L. G. Sneddon, *Chem. Mater.* **1995**, *7*, 1942–1956.
2) B. Li, C.R. Zhang, F. Cao, S.Q. Wang, Y. B. Cao, J. Feng, B. Chen, *Adv. Appl. Ceram.* **2008**, *107*, 1–3.
3) B. Li, C. R. Zhang, F. Cao, S. Q. Wang, Y. G. Jiang, *J. Inorg. Mater.* **2008**, *23*, 229–232.
4) P. X. Feng, H. X. Zhang, *Int. J. Refract. Met. Hard Mater.* **2009**, *27*, 823–828.
5) L. Maya, *Appl. Organomet. Chem.* **1996**, *10*, 175–182.
6) Q. Guo, Y. Xie, C. Yi, L. Zhu, P. Gao, *J. Solid State Chem.* **2005**, *178*, 1925–1928.
7) G. J. Qi, C. R. Zhang, H. F. Hu, *J. Non-Cryst. Solids* **2006**, *352*, 3794–3798.
8) G. J. Qi, C. R. Zhang, H. F. Hu, F. Cao, S. Q. Wang, Y. B. Cao, Y. G. Jiang, *Mater. Lett.* **2005**, *59*, 3256–3258.
9) T. Wideman, E. E. Remsen, E. Cortez, V. L. Chlanda, L. G. Sneddon, *Chem. Mater.* **1998**, *10*, 412–421.
10) http://www.chemspider.com/Chemical-Structure.122374.htm
11) David R. Lide, ed. (**2005**). *CRC Handbook of Chemistry and Physics*. Boca Raton, Florida: CRC Press.
12) E. Arunan, G. R. Desiraju, R. A. Klein, J. Sadlej, S. Scheiner, I. Alkorta, D. C. Clary, R. H. Crabtree, J. J. Dannenberg, P. Hobza, H. G. Kjaergaard, A. C. Legon, B, Mennucci, D. J. Nesbitt, *Pure Appl. Chem.* **2011**, 83, 1619.
13) K.S. Kim, P. Tarakeshwar, J.Y. Lee, *Chem. Rev***. 2000**,100,4145
14) M. Nishio, *Cryst. Eng. Commun.* **2004**,6,130.
15) H. Matsuura, H. Yoshida, M. Hieda, S. Yamanaka, T. Harada, K. Shin-ya, K. Ohno, *J. Am. Chem. Soc.* **2003**,125, 13910.
16) G. C. Pimental, A. L. McClellan, The Hydrogen Bond; W. H.Freeman: San Francisco, CA, **1960**.
17) Jeffrey, G. A.; Saenger, W. Hydrogen Bonding in Biological Structures; Springer: Berlin, **1991**
18) G. A. Jeffrey, an Introduction to Hydrogen Bonding (Oxford University Press, New York, **1997**).

19) A. E. Reed, L. A. Curtiss, F. Weinhold, *Chem. Rev*., **1988**, 88, 899–926

20) M. E. Wieser, N. Holden, T. B. Coplen, J. K. Böhlke, M. Berglund, W. A. Brand, P. De Bièvre, M. Gröning, R. D. Loss, J. Meija, T. Hirata, T. Prohaska, R. Schoenberg, G. O'Connor, T. Walczyk, S. Yoneda, X. K. Zhu, *Pure Appl. Chem.*, **2013**, 85, 1047-1078

21) E. Whittle, D. A. Dows, G. C. Pimentel, *J. Chem. Phys*. **1954**, 22, 1943

22) S. Cradock, A. J. Hinchcliffe, *Matrix Isolation, Chap. 2*, Cambridge University Press, London (**1975**).

23) H. E. Hallam, *Vibrational Spectroscopy of Trapped Species* (Wiley Inter science Publication, London, **1973**)

24) G. C. Pimentel, S. W. Charles, *Pure and Appl. Chem*. **1963**, 7, 111

25) A. D. Buckingham, *Proc. Roy. Soc*. (London) A **1958**, 248, 169

26) Spectroscopy in Inorganic Chemistry, Volume 1, edited by C.N.R. Rao

27) http://www.arscryo.com/TechNotes/CryocoolerPrincipleofOperation

28) P. R. Griffiths, J. A. Haseth, *Fourier Transform Infrared Spectrometry* (John Wiley & Sons), New York, **1986**

29) Jun-sheng Li, Chang-rui Zhang, Bin Li, Feng Cao, Si-qing Wang, *Eur. J. Inorg. Chem.* **2010**, 1763–1766

30) A. Kaldor, R. F. Porter, *Inorg. Chem.*, ***1971**, 10,775-785*

31) M. J. Frisch, G. W. Trucks, H. B. Schlegel, G. E. Scuseria, M. A. Robb, J. R. Cheeseman, G. Scalmani, V. Barone, B. Mennucci, G. A. Petersson, H. Nakatsuji, M. Caricato, X. Li, H. P. Hratchian, A. F. Izmaylov, J. Bloino, G. Zheng, J. L. Sonnenberg, M. Hada, M. Ehara, K. Toyota, R. Fukuda, J. Hasegawa, M. Ishida, T. Nakajima, Y. Honda, O. Kitao, H. Nakai, T. Vreven, J. A. Montgomery, Jr., J. E. Peralta, F. Ogliaro, M. Bearpark, J. J. Heyd, E. Brothers, K. N. Kudin, V. N. Staroverov, T. Keith, R. Kobayashi, J. Normand, K. Raghavachari, A. Rendell, J. C. Burant, S. S. Iyengar, J. Tomasi, M. Cossi, N. Rega, J. M. Millam, M. Klene, J. E. Knox, J. B. Cross, V. Bakken, C. Adamo, J. Jaramillo, R. Gomperts, R. E. Stratmann, O. Yazyev, A. J. Austin, R. Cammi, C. Pomelli, J. W. Ochterski, R. L. Martin, K. Morokuma, V. G. Zakrzewski, G. A. Voth, P. Salvador, J. J. Dannenberg, S. Dapprich, A. D. Daniels, O. Farkas, J. B. Foresman, J. V. Ortiz, J. Cioslowski, and D. J. Fox, Gaussian, Inc., Wallingford CT, **2010**

32) S. F. Boys, F. Bernadi, Mol. Phys., **1970**, 19, 553

33) R.F.W. Bader, Atoms in Molecules. A Quantum Theory, ClarendonOxford, **1994**.

34) R. G. A. Bone, R.F.W. Bader, *J. Phys. Chem*. **1996**, 102, 10892
35) F. Biegle-Koning, R.F.W. Bader, W. H. Tang, J. Comput. Chem**. 2000,** 96, 6796 (AIM 2000, Version 1).
36) R.M. Bentwood, A.J. Barnes, W.J. Orville-Thomas, *J. Mol. Spec.* **1980**, 84, 391–340
37) J. Wu, H. Yan, H. Chen, G. Dai, A. Zhong; Computational and Theoretical Chemistry, **2012,** 984, 51-56
38) Y. S. Al-Hamdani, D. Alfe, O. Anatole von Lilienfeld, A. Michaelides, *J. Chem. Phys*. **2014** 141, 18C530
39) P. Malla, D. Marion, E. V. Ivanova, H. M. Muchall, *J. Mol. Str.*, **2010**, 979, 101-107
40) K. Sankaran, K. Sundararajan, K. S. Viswanathan, *J. Mol. Str.* **2002,** 609, 177-185
41) B. S. Ault; G. C. Pimentel**;** *The dournai of Physicai Chemistry,***1975,** 79, 621-626
42) A. Engdahl, B. Nelander, *J. Phys. Chem.*, **1985,** 89, 2860-2864
43) H. S. Gutowsky, T. Emilsson, E. Arunan, *J. Chem. Phys.*,**1993,** 99, 4883-4893